(Received 29 July 2025, Accepted 4 September 2025, Scheduled 11 September 2025)

Design of a Miniaturized Dual Notched UWB Bandpass Filter Using Meander Resonator with C-Band Interference Suppression Capability

Piali Chakraborty[1, *], Jyoti Ranjan Panda[2], Arindam Deb[3], and Jibendu Sekhar Roy[2]

[1] *Department of Electronics and Communication Engineering, Rajeev Institute of Technology, Karnataka, India*
[2] *School of Electronics Engineering, KIIT Deemed to be University, Bhubaneswar, India*
[3] *Sisir Radar Pvt Ltd., Kolkata, India*

ABSTRACT: This article proposes a miniaturized dual notched ultrawide bandpass filter (BPF) for ultra-wideband (UWB) indoor applications. The initial operational spectrum recognition is realized through the resonances of multiple mode resonator (MMR). Then, both the passband and stopband characteristics are improved substantially by mounting distinctly shaped meander resonators cascaded with open loop ring resonator on the MMR. Further, the interdigital coupled lines are also meandered to contribute in filter size reduction along with tightening the coupling between the effective filter structure and input/output ports. The elimination of interfering signals within the passband caused by C-band satellite downlink and fixed satellite service uplink is facilitated by two sharp notches at 3.76 GHz and 6.82 GHz frequencies. Concurrently, this miniaturized filter is also characterized by its wide passband of 6.42 GHz with fractional bandwidth (FBW) 110.88%, good selectivity of 0.85, minimal insertion loss differing between 0.44 dB and 0.85 dB, wide upper stopband of 5.11 GHz, etc. ensuring its suitability as a practical UWB filter. The design is fabricated and measured to compare with the simulated outcomes and validated by the obtained resemblance between the measured and simulated filter outputs.

1. INTRODUCTION

Recently, every aspect of our lives has been ubiquitously influenced by the applications of wireless communication systems. Nowadays, we are using a hefty of different internet of things (IoT) and portable devices to perform many automated tasks along with conventional cellular communications and other wireless services. Day by day, these devices and antennas are getting smaller in size, demanding cost-effective, lightweight, and highly miniaturized circuits. On the other hand, the progress in technology has been increasing the number of users sharply. As a result, spectrum congestion and interference issues have also risen simultaneously. Therefore, not only developing compact circuits but eliminating interference has also become a prime concern for researchers. At this current juncture, the assignment of the 3.1–10.6 GHz spectrum by Federal Communications Commissions (FCC) for unlicensed ultra-wideband applications has unfolded an immense opportunity to develop compact, low-cost UWB antennas and filters having high bandwidth and gain [1]. UWB bandpass filters are an indispensable part of the UWB system. Filters are also used in filtering antennas [2–4] where filters are integrated with antennas.

Numerous techniques have been introduced by researchers thereafter to design UWB filters. Initially, parallel coupled resonators were used to realize transmission zeros at passband edges, but the main drawback of this kind of filter was their large size and narrow stopband [5]. Cascading high pass and low pass filters partially resolved the signal interference problem that prevailed due to narrow stopbands, though the issues related to large size and high insertion loss still lingered [6]. Meanwhile, the development in design based on applying multiple mode resonator (MMR) structure and microstrip to coplanar waveguide transition technology came into view as the solution to the above problems [7, 8]. Due to design simplicity and flexibility in allocating its leading resonant modes to form the passband, MMR method is perhaps the most convenient method. UWB signals with large bandwidths (3.1 GHz–10.6 GHz) coexist with licensed radio services like WiMAX (2.3, 2.5, 3.5 GHz), WLAN (5, 5.85 $\sim$ 5.925 GHz), Wi-Fi (6 GHz), C band (4 $\sim$ 8 GHz), X band (8 $\sim$ 12 GHz), and satellite communication (8 GHz), so the focus of the recent research activities in this field is on measures to minimize interference effects. This purpose is served by the notches introduced in the passband at desired frequencies or by developing multiband filters and placing stopband at the desired frequency. Available notch-generating techniques are reviewed intensively and discussed below.

The UWB antenna designed by the authors in [9] comprises four fractal-shaped circular radiators connected with a tapered feedline placed orthogonally on the top plane. The bottom plane has partial ground connected to antenna elements through parasitic elements, which contributes to good isolation. An asymmetric tri-step stepped impedance resonator (ATSSIR) has been introduced in [10] to develop a UWB bandpass filter.

* Corresponding author: Piali Chakraborty (chakraborty.piali1987@gmail.com).

Additionally, loading two stepped impedance stubs and one shorted stub to the ATSSIR facilitates a notch at 5 GHz to mitigate WLAN interference. In [11], initially, the UWB bandpass filter is formed by three short-circuited quarter-wavelength stubs mounted to the transmission line, and they are separated from each other by a half-wavelength distance. To dismiss the interference produced by WLAN devices, a notch at 5.5 GHz has been developed by converting the short-circuited stubs into exponentially tapered impedance line stubs. The bandpass filter structure in [12] consists of U-shaped resonators shorted with microstrip lines on the top surface and slotted semi-ellipse coplanar waveguide (CPW) on the bottom. The addition of open-circuited stubs to the microstrip line on the top surface is utilized to circumvent the X-band satellite downlink frequency at 7 GHz. The authors in [13] have designed a bandpass filter by employing defected ground structure (DGS) units, low-impedance microstrip lines, and quasi-interdigital capacitors. Each DGS unit has two isosceles right triangles joined by straight slots. Filter performance is enhanced by two notches at 7.8 and 5.5 GHz produced by the meander line slot and folded coupling arm, respectively. In [14], the authors have designed a CPW in butterfly shape on the ground plane. Implementing surface-to-surface transition technology, microstrip lines on top surface are amalgamated with folded split ring resonators (FSRRs) to generate a UWB notched bandpass filter. Two notches at 6.1 and 8.1 GHz are produced to remove the C-band and X-band interferences, respectively. A compact wideband bandpass filter has been presented in [15] where the ring resonator is rectangular and stub-loaded. Later performance enhancement is realized by modifying the structure into a novel asymmetric structure, resulting in four notches in the passband at 4.34, 5.48, 6, and 9.3 GHz, alleviating interference caused by S-band radar, WLAN, Wi-Fi 6E, and X band radar signals, respectively. In [16], an elliptical split ring resonator (SRR) has been embedded as the integrated part of a distinctly shaped ring that is mounted on an MMR. This configuration is able to facilitate two notches or three notches in the passband of this UWB BPF by changing only the axial ratio of SRR. For double-notched filter, WLAN (wireless local area network) and satellite communication signals are suppressed by the notches occurring at 5.58 and 8.06 GHz. On the other hand, for triple-notched filters, notches that emerged at 5.48, 7.68, and 8.82 GHz can efficiently remove the interference from WLAN, C-band, and X-band radar, respectively. In [17], an elliptical monopole radiator is embedded with a stepped impedance stub-loaded MMR-based bandpass filter to develop a reconfigurable filtenna. The filtenna is tuned to operate in two states, namely the UWB state for spectrum sensing and the C band for communication in a cognitive radio environment, by employing two PIN diodes.

In latest research articles, the application of meander lines has gained focus to generate miniaturized filters or antennas. For instance, in [18], a triple-passband negative group delay filter has been presented, where the compact size of the filter is obtained by converting the conventional step impedance resonator (SIR) into a meander step impedance resonator (MSIR). In [19], a multiband antenna is realized by removing slots in the bottom plane beneath the microstrip transmission line on the top surface. Gain enhancement of the antenna is obtained by introducing fractalized uniplanar meander line electromagnetic band gap (EBG) surrounding the microstrip line. The bandgap of the EBG lies in the WiMAX (3.6 GHz) and WLAN (5.2 GHz) bands. In [20], adjustable wideband and multiband antennas have been presented, applying slot meander patch concept for 4G long-term evolution handheld devices. The authors in [21] have designed a miniaturized dual-band bandpass filter by integrating a bandstop filter and a bandpass filter. The bandpass filter comprises SIR along with a coupling structure, and the bandstop filter is constructed by a T-shaped line integrated with meander lines.

Taking into account the overall filter size reduction and performance enhancement capability of meander lines, this article presents a new design approach for a compact UWB bandpass filter employing distinctly shaped meander resonators. Meander resonators cascaded with an open loop ring resonator are mounted on the MMR. Meandered interdigital coupled lines also play a part in filter size reduction. Two notches possessing high rejection ability are introduced in the passband by this filter configuration. In this work, the proposed design is simulated in High Frequency Structure Simulator (HFSS) software using an Arlon AD250C substrate having a thickness of 0.76 mm, a relative permittivity of 2.5, and a loss tangent of 0.0015 [22]. Here, Section 2 discusses the proposed design of the filter and its equivalent circuit analysis. Section 3 demonstrates the simulated performance of the proposed filters along with the significance of the meander resonator in the proposed design. Section 4 shows the measured results, and Section 5 draws the conclusion.

2. DESIGN OF DUAL NOTCHED FILTER

2.1. Design of Notched Band UWB BPF

An ultrawide bandpass filter is configured first by employing MMR and aperture-backed interdigital coupled lines connected to incoming/outgoing feed lines, as depicted in Fig. 1(a). High impedance lines of the MMR along with interdigital coupled lines are meandered by bending them in a 'Z' shape, resulting in an overall reduction in the filter size. Next, inverse 'L'-shaped slots are cut from the ground plane below the interdigital coupled arms, ensuring a tight coupling between feedlines and the filter structure. The basic ultrawide bandpass filter developed by the design presented in Fig. 1(a) is revamped as depicted in Fig. 1(b). Two open-loop new distinctly shaped meander resonators and one open-loop ring resonator of a particular shape are cascaded in series. Thus, a compact structure is formed, and this whole structure is mounted on the MMR through two vertical stubs. This compact layout not only enhances the filter performance by inducing high selectivity and increasing the width of both the passband and stopband but also generates two notches in the passband at 3.76 GHz and 6.82 GHz to discard the C band satellite downlink signal and fixed satellite service uplink signal, respectively. For further improvement in terms of loss reduction, three open-ended stubs are suspended from three cascaded resonators.

The ultimate shape and dimensions of the ring resonator and meander resonators are obtained after conducting a large num-

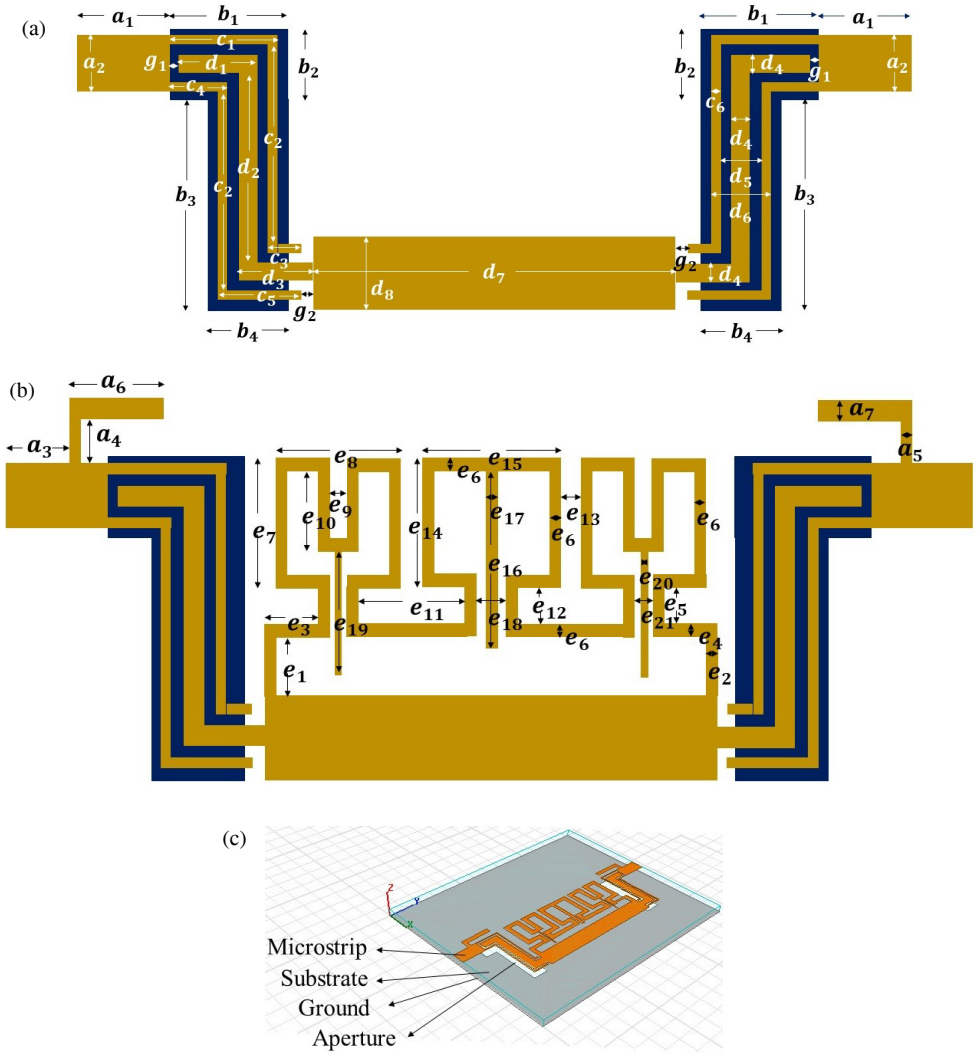

FIGURE 1. Proposed UWB BPF. (a) MMR based basic configuration, (b) notched band structure using meander resonator, (c) perspective view.

ber of simulation studies. Optimum dimensions (in mm) of the filter referring to Fig. 1 are mentioned in Table 1.

2.2. Chronological Formation of the Filter

The progressive evolution process of the filter, proposed in this article, is portrayed explicitly in Fig. 2. Performance comparison in terms of $|S_{21}|$ characteristic related to each stage is explained in Fig. 3. In the first step, an MMR is coupled to the input/output port through aperture-backed interdigital coupled lines, resulting in a bandpass response having a 6.82 GHz wide passband at 3 dB and a 4.03 GHz wide stopband with a 15 dB attenuation level. Though the passband resulting from three resonant modes is wide, the transition bands obtained in this step are not sharp. In the second step, corresponding to Fig. 2(b), two microstrip meander open loop resonators at two sides and one open loop ring resonator in the middle are joined to each other, and the resulting structure is connected to the MMR by two vertical stubs. This step generates one transmission zero at 2.43 GHz, i.e., the lower edge of the passband, and the other at 10.1 GHz, i.e., the upper edge of the passband, causing a rapid switch between in-band and out-of-band. Moreover, two notches are also introduced in the passband at 3.76 GHz and 7.12 GHz, but further improvement is needed because of poor stopband characteristics and a high insertion loss of 3.75 dB in the passband. In the third step, as shown in Fig. 2(c), open-ended bent stubs are loaded to feed lines, broadening the upper stopband width to 4.47 GHz. A suspended stub, connected to the ring resonator, located in the middle of the cascaded structure in the fourth step, assists in reducing the passband insertion loss as shown in Fig. 2(d). Finally, Fig. 2(e) presents the complete design of the proposed filter. In this step, another two vertical stubs are suspended from the two meander resonators located on both sides of the ring resonator to produce a passband with minimized insertion loss. The second notch occurs at 6.82 GHz by slight left shifting while the sharpness and attenuation level of both the notches are increased to a certain degree.

2.3. Equivalent Circuit Analysis

Due to symmetry, the filter structure can be separated into odd and even modes for analysis, as depicted in Fig. 4. Resonances of the simulated design appear at 3.1, 4.62, 6.72, and

TABLE 1. Proposed filter dimensions.

Parameters	VALUE (MM)	Parameters	Value (mm)	Parameters	Value (mm)	Symbol Parameters	Value (mm)
a_1	3	c_3	0.48	d_8	2.1	e_{10}	2.5
a_2	1.6	c_4	1.4	$d = d_1 + d_2 + d_3$	9.22	e_{11}	3.2
a_3	2	c_5	1.94	g_1	0.21	e_{12}	0.5
a_4	0.65	c_6	0.14	g_2	0.21	e_{13}	0.5
a_5	0.4	$c = c_1 + c_2 + c_3$	9.22	e_1	0.96	e_{14}	4
a_6	3.5	$= c_2 + c_4 + c_5$		e_2	0.5	e_{15}	4.3
a_7	0.5	d_1	2.3	e_3	2.09	e_{16}	4.7
b_1	3.06	d_2	5.12	e_4	0.34	e_{17}	0.4
b_2	1.8	d_3	1.8	e_5	0.66	e_{18}	0.8
b_3	5.76	d_4	0.9	e_6	0.5	e_{19}	2.7
b_4	1.82	d_5	1.32	e_7	4	e_{20}	0.15
c_1	2.86	d_6	1.6	e_8	4.5	e_{21}	0.5
c_2	5.88	d_7	15.48	e_9	0.5	e_{10}	2.5

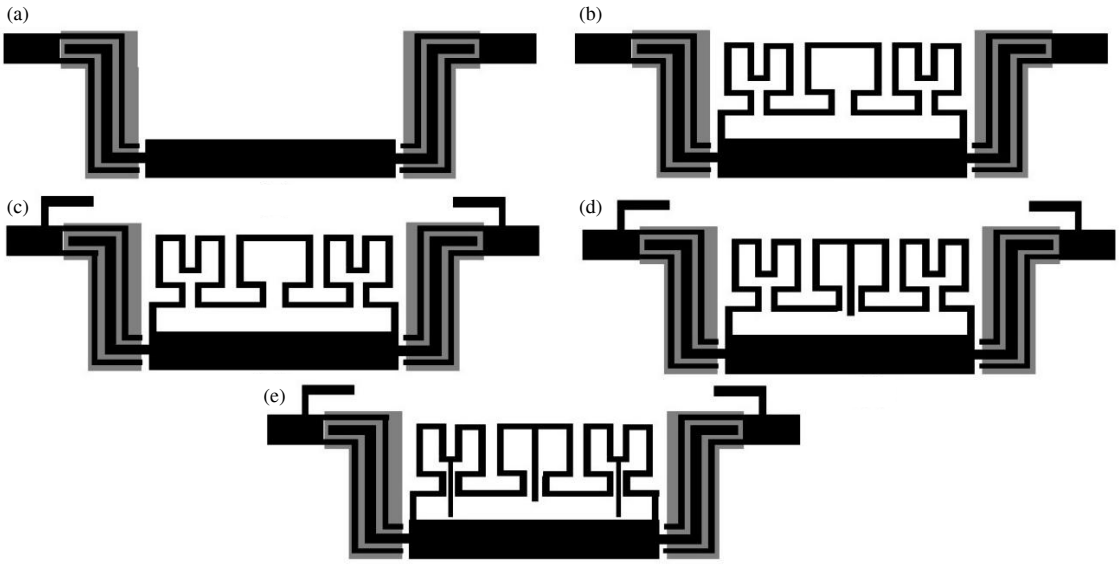

FIGURE 2. Progressive stages of filter formation, (a) step 1, (b) step 2, (c) step 3, (d) step 4, (e) step 5.

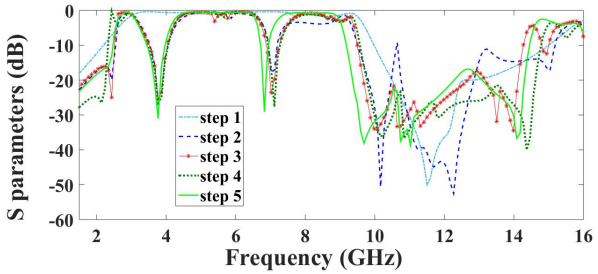

FIGURE 3. Step-wise $|S_{21}|$ response comparison.

8.25 GHz. Input admittances related to odd mode and even mode are marked as $Y_{in,odd}$ and $Y_{in,even}$. Each transmission line section in Fig. 4 is recognized by its electrical length θ and characteristic admittance Y, respectively, which can be calculated using the dimensions of the respective lines as given in Table 1. The length of the compact cascaded structure is considered as $2l$, where $l = e_3 + 3e_{12} + 2e_8 - e_9 + 2e_7 + 2e_{10} + e_{11} + e_{14} + e_{15}/2 + e_{16} + e_{19}$.

Equations that express $Y_{in,odd}$ and $Y_{in,even}$ are given below [23]. Simplification of $Y_{in,odd}$ includes Equations (1)–(2), and simplification of $Y_{in,even}$ includes Equations (3)–(8).

The maximum and minimum variations of odd mode frequency f_{o1} in Fig. 5 (a) are 250 MHz and 120 MHz. For odd mode frequency f_{o2}, these variations are 460 MHz and 160 MHz, respectively. In Fig. 5(b), the maximum and minimum variations for even mode frequency f_{e1} are 40 MHz and 0. The variations are minimal for even mode frequencies f_{e2}. Similarly in Fig. 5(c), the maximum and minimum variations of frequency in even mode frequency f_{e1} are 80 MHz and 40 MHz. For even mode frequency f_{e2}, maximum and minimum variations are 80 MHz and 0. All these variations are within the bandwidth of the filter.

$$Y_{in,odd} = Y_1(Y_{in2} + jY_1 \tan\theta_1)/(Y_1 + jY_{in2} \tan\theta_1) \quad (1)$$

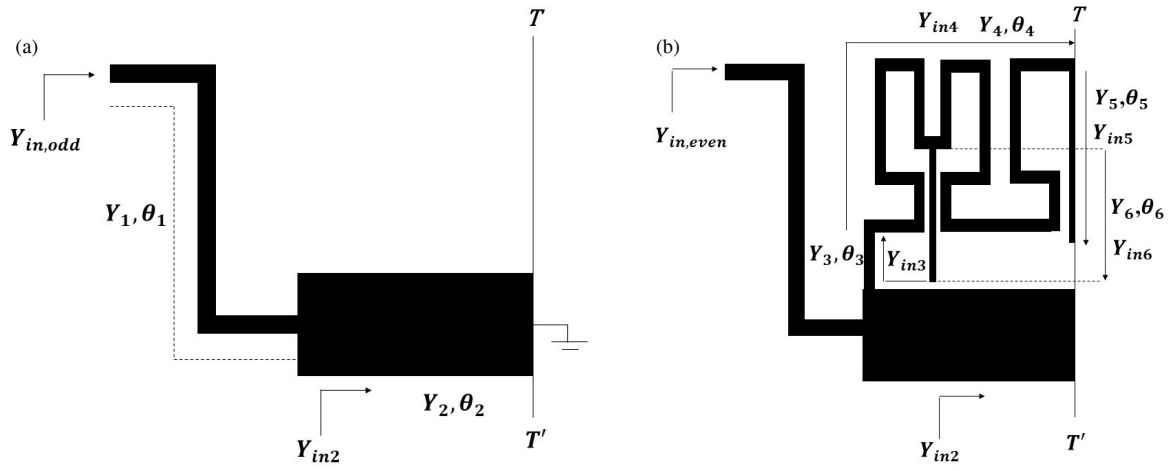

FIGURE 4. Equivalent circuit of the compact cascaded structure loaded on MMR, (a) odd mode, (b) even mode.

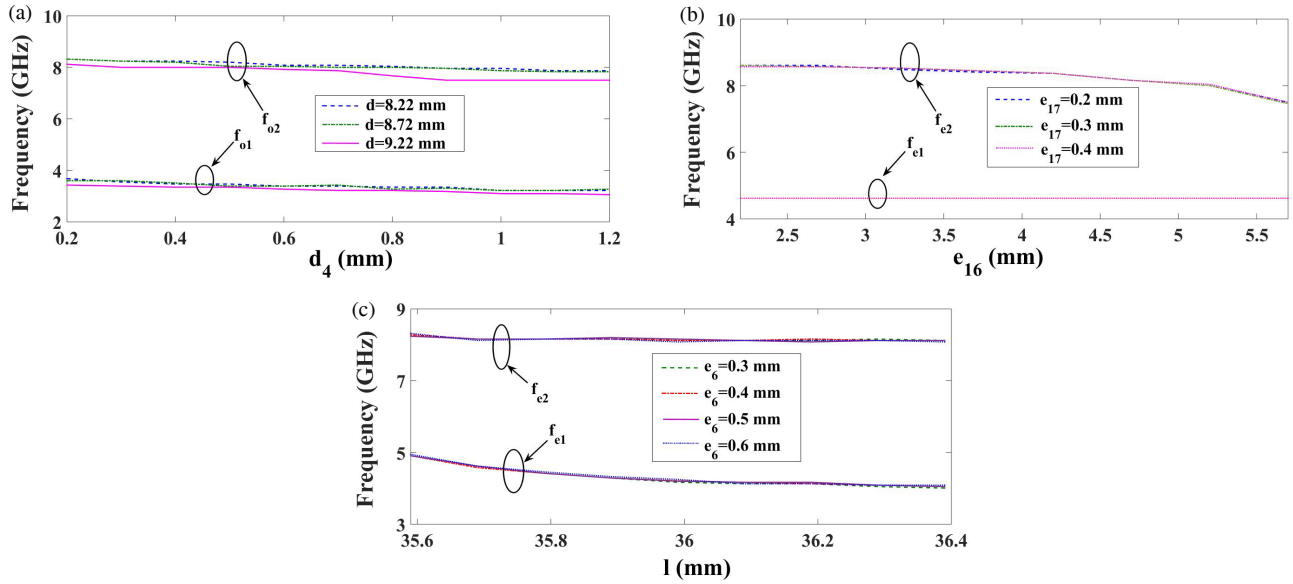

FIGURE 5. Response of the resonant frequencies varying with resonator dimensions, (a) odd mode (b), (c) even mode.

Where,

$$Y_{in2} = -jY_2 \cot\theta_2 \quad (2)$$

$$Y_{in,even} = Y_1(Y_{in2} + jY_1 \tan\theta_1)/(Y_1 + jY_{in2} \tan\theta_1) \quad (3)$$

Where,

$$Y_{in2} = Y_2(Y_{in3} + jY_2 \tan\theta_2)/(Y_2 + jY_{in3} \tan\theta_2) \quad (4)$$

$$Y_{in3} = Y_3(Y_{in4} + jY_3 \tan\theta_3)/(Y_3 + jY_{in4} \tan\theta_3) \quad (5)$$

$$Y_{in4} = Y_4(Y_{in5} + jY_4 \tan\theta_4)/(Y_4 + jY_{in5} \tan\theta_4) \quad (6)$$

$$Y_{in5} = Y_5(Y_{in6} + jY_5 \tan\theta_5)/(Y_5 + jY_{in6} \tan\theta_5) \quad (7)$$

and,

$$Y_{in6} = jY_6 \tan\theta_6 \quad (8)$$

Two odd mode resonances, such as f_{o1}, f_{o2}, and two even mode resonances, namely, f_{e1}, f_{e2}, are obtained by evaluating the aforementioned equations. Calculated resonant peaks are close to the resonant frequencies obtained in simulation, and thus the design is substantiated. The impact of high-impedance line sections (length = 'd', width = 'd_4') of the MMR on odd mode resonances is described in Fig. 5(a). For three different values of length 'd' (8.22 mm, 8.72 mm, and 9.22 mm), variations of f_{o1} and f_{o2} are observed by changing the width 'd_4' from 0.2 mm to 1.2 mm. While the design is simulated in software, values of 'd' and 'd_4' are optimized at 9.22 mm and 0.9 mm. Fig. 5(a) also depicts that there is a close match between simulated and calculated odd mode resonances for this particular length and width. Next, Fig. 5(b) and Fig. 5(c) describe the characteristics of even mode resonances. It is noted from Fig. 5(b) that f_{e2} varies with the open-ended stub of length e_{16} and width e_{17}. However, the other even mode resonance f_{e1} does not vary with this stub. On the other hand, the value of f_{e1} varies with the length $(2l)$ and width (e_6) of the compact cascaded structure, as shown in Fig. 5(c). The length has a crucial effect on f_{e1}; below 35.59 mm and above 36.39 mm, the peak f_{e1} disappears.

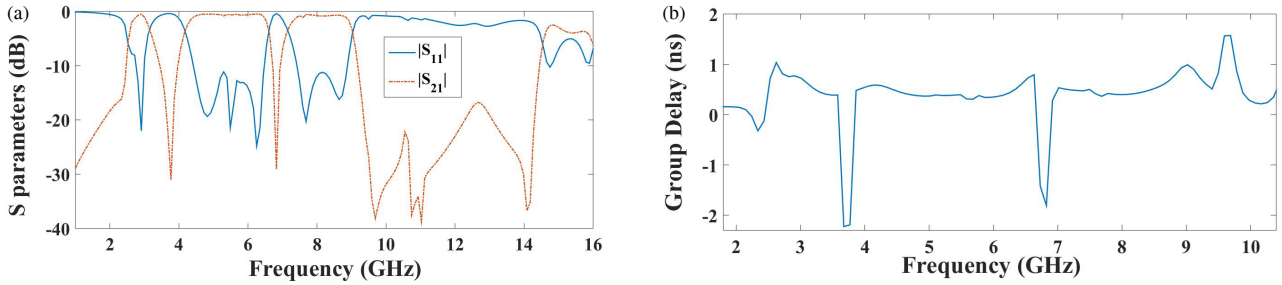

FIGURE 6. Simulated outputs of dual notched UWB bandpass filter, (a) S parameters, (b) group delay.

3. SIMULATION RESULTS

3.1. Performance of the Notched UWB Filter

Band characteristics of the presented filter are elucidated in Fig. 6(a) by S parameters. This filter has produced a 6.42 GHz wide passband ranging between 2.58 GHz and 9 GHz. $|S_{21}|$ characteristic depicts a low insertion loss varying within a range of 0.44 dB to 0.85 dB. The input reflection coefficient value is -11.21 dB, which is much lower than -10 dB as per the FCC specified standard. Moreover, the passband characteristic is enriched by two notches appearing at 3.76 GHz and 6.82 GHz, possessing deep suppression levels of 31 dB and 29 dB, respectively. The first notch has an FBW of 28.26%, and the second notch has an FBW of 8.5%, both measured at 3 dB. Concurrently, the lower stopband width is 1.6 GHz, and the upper stopband width is 5.11 GHz (ranging from 9.27 GHz to 14.38 GHz). The upper stopband has a high rejection capability with an attenuation level of 16.73 dB. Besides, the group delay variation throughout the passband is also small, i.e., 0.32 ns to 0.76 ns, excluding the notch frequencies as portrayed in Fig. 6(b). The proposed dual-notched bandpass filter consumes an area of $1.02\lambda_g \times 0.32\lambda_g$.

Following observing the resonance characteristics and band characteristics, the essentiality of applying apertures on the ground plane underneath the interdigital coupled line is reported in Fig. 7. Correctly placed and shaped apertures can influence the filter performance eminently. A tight coupling between the interdigital coupled arms and the effective filter structure in the presence of apertures ensures the transferring of maximum power and minimization of signal reflection from the input port. Fig. 7 demonstrates a considerable degradation of the passband uniformity both for $|S_{11}|$ and $|S_{21}|$ characteristics in the absence of apertures.

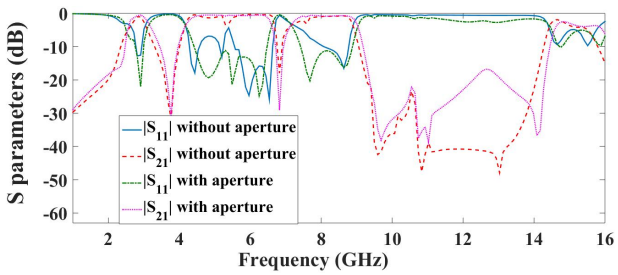

FIGURE 7. Magnitude of S parameters for dual notched UWB bandpass filter without and with apertures.

Next, the surface current distribution patterns through the filter at two notch frequencies and cutoff frequencies are displayed in Fig. 8. At notch frequencies such as 3.76 GHz and 6.82 GHz, meander resonators and ring resonator hold the maximum surface current density. On the other hand, at lower (2.58 GHz) and upper (9 GHz) cut-off frequencies, feed lines in both the input/output sides and interdigital couple lines have substantial surface current density.

3.2. Performance Analysis of the Meander Resonator

To evaluate the efficacy of meander resonators in the overall filter performance improvement in terms of $|S_{21}|$ characteristic, a parametric examination is conducted in this section. First, Fig. 9 depicts the transformation of a straight transmission line into a meander transmission line. Meander lines are the close-packed version of the straight line, providing similar output responses and thus allowing a reduction in circuit size. Bends in meander lines cause a reduction in inductance in that area, and this reduction is compensated by increasing line length. By applying this approach, a new meander resonator is designed, and a cascaded form of open-loop meander resonators and open-loop ring resonators is composed. The comparative responses between the outcomes throughout the passband and stopband of the filter with and without employing the meandering approach are explained in Fig. 10. It is inferred that in parameters like selectivity of the passband, insertion loss, and sharpness of the notches, the filter outputs are improved to a certain degree due to the utilization of meandering approach.

In this context, it is mentioned that the filter discussed in the proposed article is a microstrip filter. Generally, in a microstrip filter, when the electromagnetic waves flow through different paths, they can interfere and cancel each other out. Thus, at a specific frequency or at a narrow band of frequency, no signal is transmitted, and that frequency is known as a notch. The process of generation of notches can be varied in different types of microstrip filters. A notch can appear in a coupled line filter if the signal propagation path undergoes a 180-degree phase shift at a certain frequency, and the signals are cancelled out at the output. On the other hand, in the microstrip filters having multiple resonators, for instance, stub-loaded resonators, hairpin resonators, and parallel-coupled line resonators, a transmission zero, hence a notch, can emerge due to coupling between non-adjacent elements. Furthermore, introducing short-circuited or open-circuited stubs in the structure of a microstrip filter can form a notch in the passband, as the change of impedances of

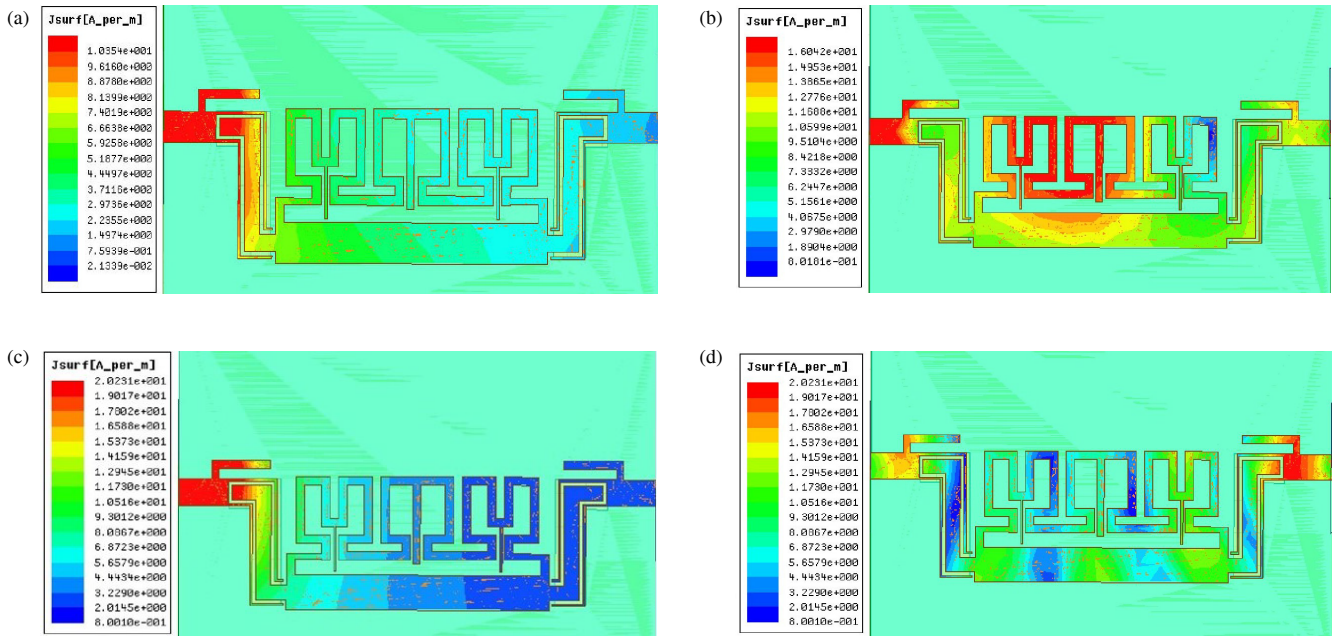

FIGURE 8. Surface current distribution in dual notched UWB bandpass filters at (a) 3.76 GHz (b) 6.82 GHz (c) 2.58 GHz (d) 9 GHz.

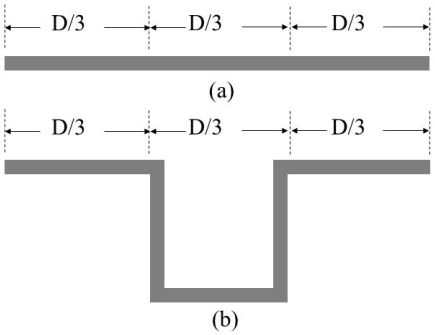

FIGURE 9. Geometry of (a) straight transmission line (b) meander transmission line.

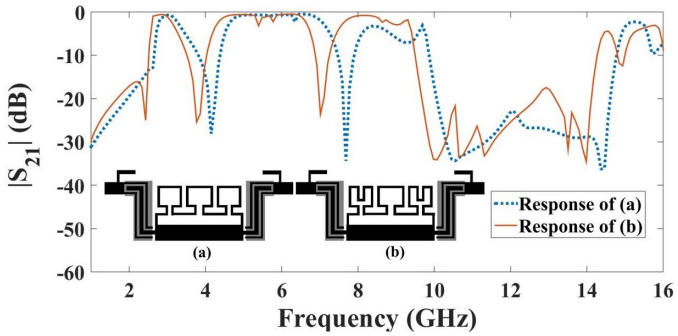

FIGURE 10. Magnitude of $|S_{21}|$ without (Figure (a) in inset) and with (Figure (b) in inset) applying meander line.

the stubs can cause interference in the signal path. Additionally, etching on the ground plane beneath the microstrip line can create a notch by reflecting energy at resonant frequency. Also, notches can be formed due to structural asymmetry of the resonators or parasitic coupling between resonators or feed lines.

A comparison between the obtained band characteristics of the proposed filter and the available related recent filters in the literature is reported in Table 2. Here, column-wise table entries indicate reference number, brief description of filter composition, dielectric constant/thickness of the substrate used, passband span, insertion loss, upper stopband width with attenuation, number of notches, center frequency of the notch with attenuation, and filter size measured in guided wavelength calculated at center frequency. All simulation works of the proposed filter are operated on 6.85 GHz, taking guided wavelength (λg) as 27.69 mm. The structure proposed in this article is more compact in size than other structures [10, 11, 14, 24, 27–29, 31, 32]. The bandwidths achieved for passband are much less in some designs [21, 30]. Also, the narrow stopband in [21] prevents the proper isolation of desired signals from higher-order frequencies. Further, the attenuation level of the stopband is very low in [25]. Also, the insertion loss appearing in the passband is high in [26] compared to the proposed filter. The filter size reduction and performance enhancement capability of meander lines are successfully utilized in this article through a new and compact design. A meander resonator of distinct-shape integrated with MMR is presented here. Interdigital coupled lines are also meandered.

4. MEASURED RESULTS

Arlon AD250C substrate is used for fabrication of the designed filter, as exhibited in Fig. 11. Fig. 12 provides a comparison between the simulated and measured results. A considerable resemblance is observed between the simulated and measured outputs for both S parameters and group delay plots. The coupling effects of different elements over the frequency are dif-

TABLE 2. Comparison of proposed filter attributes with the contemporary published papers.

Ref.	Filter composition	ε_r/t (mm)	Passband (GHz)	Insertion Loss (dB)	USB (GHz)/ Attenuation (dB)	No of notches	Notch frequency (GHz)/attenuation (dB)	Filter size ($\lambda_g \times \lambda_g$)
[10]	Multi stubs loaded asymmetric tri-step SIR	2.2/0.787	3.1–11.02	< 1	4.5/15	1	5/> 40	0.67×0.46
[11]	Microstrip resonator loaded with exponentially tapered impedance line stubs	4.4/1.6	2.7–11	< 3	0.5/10	1	5.5/32	1.48×0.53
[14]	Microstrip line with folded SRRs and butterfly shaped CPW	4.4/0.8	2.75–10.7	0.87–1.8	7/15.8	2	6.1/> 15.5, 8.1/> 15.5	1.01×0.76
[21]	SIR having meandered high impedance line, folded structure, and T shaped meander line	2.54/0.54	2.15–4.5	0.024	3/17	1	3.75/45	0.42×0.29
[24]	T shaped resonator placed close to transmission line having L shaped defect microstrip structure	2.2/1	2.62–10.62	0.8	NA	2	3.5/25.2, 7.5/17.3	1.08×0.34
[25]	Two pairs of high impedance half wavelength resonators	2.2/0.787	3.4–10	0.7–2.4	9/10	1	5.2/22.7	0.8×0.32
[26]	π resonator and LC resonator attached to suspended strip line	3.55/0.254	2.9–10.6	< 1.3	3.5/27	1	5.82/19	0.34×0.73
[27]	SIW based filter with conventional and dual split square complementary SRRs	4.3/1.6	2.9–10.3	0.7–1.84	4/20	1	5.46/> 14	0.35×1.06
[28]	Double T-shaped MMR, folded SRRs, and complementary SRRs	3.38/0.8	3.5–10.1	0.86–1.3	6/20	2	5.8/14, 8/> 16	1.66×0.75
[29]	MMR, stub loaded SIR, DGS, coupled folded arm resonator	4.3/1.62	3.3–9.75	0.8	8.5/13	1	6.2/24	1.35×0.54
[30]	Radial stubs attached with SIR	3.66/0.508	5.35–6.64	1.12	6/> 40	NA	NA	0.385×0.295
[31]	multi-layer structure of microstrip-slot wire-microstrip wide edge coupling	3.38/0.508	3.7–7.5	< 1.5	12.5/10.5	NA	NA	0.5×0.93
[32]	Transmission lines and Modified-Minkowski resonators are employed	3.5/1.5	5–11	0.26-1	NA	3	5/23, 5.98/25, 11/23.5	0.85×0.54
[This work]	MMR loaded with cascaded structure having meander resonators and ring resonator	2.5/0.76	2.58–9	0.44–0.85	5.11/16.73	2	3.76/31, 6.82/29	1.02×0.32

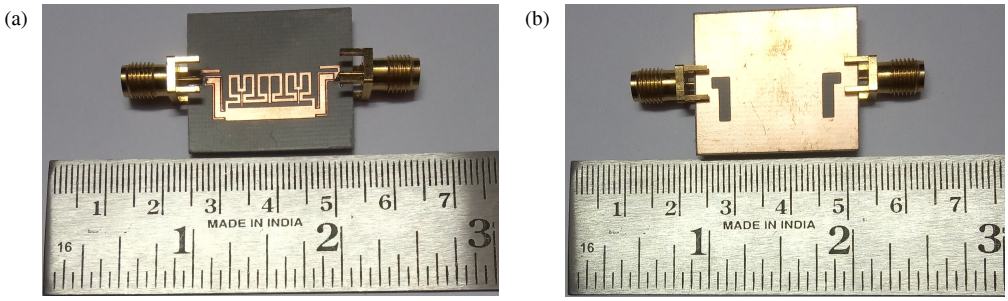

FIGURE 11. View of the dual-notched bandpass filter after fabrication, (a) top, (b) bottom.

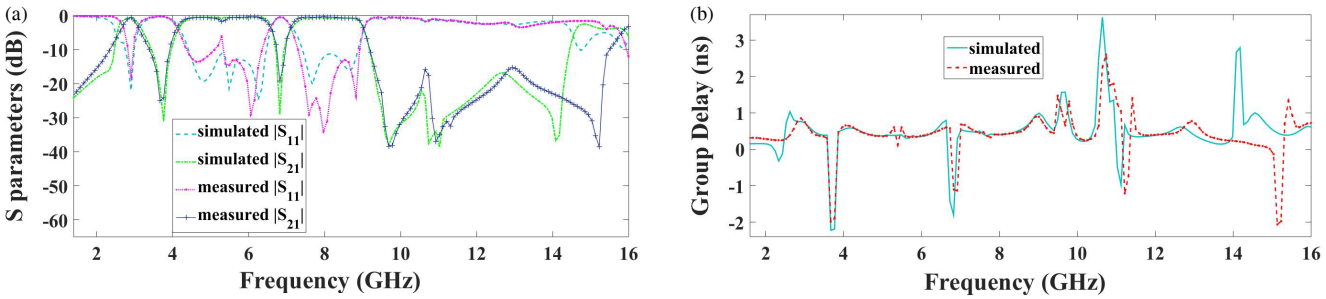

FIGURE 12. Comparison between simulated and measured outcomes, (a) S parameters, (b) group delay.

ferent, which impacts notch bandwidth. Also, the power loss occurring due to the metal (ohmic) loss in feed line, while attaching feed to SMA connector, results in an insertion loss near the lower edge of the passband. Thus, notch formed near the lower edge of the passband is also affected by this loss, but in the case of second notch this work has achieved a noticeable narrowness.

5. CONCLUSION

This article comes up with a new design approach of a dual-notched miniaturized ultra-wideband bandpass filter employing a combination of components such as MMR, interdigital coupled lines, an open-loop ring resonator, new particularly shaped meander resonators, and vertical stubs. The proposed filter structure is a combined structure where spacing gaps between the different lines are different, and the microstrip line widths are also different in different places in the filter structure. Therefore, it is difficult to determine the coupling coefficient in the whole structure. However, the impact of the coupling coefficients between different line segments is considered to present the characteristics of the proposed filter in simulated and measured outcomes of S parameters and group delay (Fig. 12). The external quality factor of a filter represents how effectively the designed filter couples to the external circuits, which represents the energy lost to the external circuits per cycle. In this work, the filter is designed but not used for any external circuit. Therefore, the information of external quality factor is not provided.

The proposed notched filter has exhibited its superiority in suppressing the coexisting authorized radio frequency (RF) interferences that appeared in the passband due to the C-band satellite downlink signal and fixed satellite service uplink signal by producing two sharp notches at frequencies of 3.76 GHz and 6.82 GHz having FBWs of 28.26% and 8.5%, respectively. The passband attained by this designed filter is 6.42 GHz, with the FBW of 110.88%. Apart from that, an upper stopband of 5.11 GHz with an attenuation level of 16.73 dB is achieved, where a 2.92 GHz stopband adjacent to the upper edge of the passband ensures isolation by suppressing higher-order spurious frequencies up to 20 dB. Moreover, the other features like return loss of 11.21 dB, insertion loss varying minimally between 0.44 dB and 0.85 dB, a high value of selectivity, i.e., 0.85 computed at 20 dB, compactness in size $(1.02\lambda_g \times 0.32\lambda_g)$, etc. prove the pertinence of the design to UWB applications.

REFERENCES

[1] Federal Communications Commission, "Revision of part 15 of the commission's rules regarding ultra-wideband transmission systems," First Report and Order, FCC 02. V48, Apr. 2002.

[2] Abdel-Jabbar, H., A. S. Kadhim, A. L. Saleh, Y. I. A. Al-Yasir, N. O. Parchin, and R. A. Abd-Alhameed, "Design and optimization of microstrip filtering antenna with modified shaped slots and SIR filter to improve the impedance bandwidth," *Telkomnika*, Vol. 18, No. 1, 545–551, 2020.

[3] Boddu, R., A. Deb, and J. S. Roy, "Design of a microstrip filtering antenna for 4G and 5G wireless networks," *Journal of Telecommunications and Information Technology*, Vol. 2023, No. 2, 78–83, 2023.

[4] Boddu, R., A. Deb, and J. S. Roy, "Design of a compact microstrip filtenna for miniaturized devices to access Internet of Things using long term evolution," *Advanced Electromagnetics*, Vol. 12, No. 4, 10–16, Dec. 2023.

[5] Shaman, H. and J.-S. Hong, "A novel ultra-wideband (UWB) bandpass filter (BPF) with pairs of transmission zeroes," *IEEE*

Microwave and Wireless Components Letters, Vol. 17, No. 2, 121–123, Feb. 2007.

[6] Gomez-Garcia, R. and J. I. Alonso, "Systematic method for the exact synthesis of ultra-wideband filtering responses using high-pass and low-pass sections," *IEEE Transactions on Microwave Theory and Techniques*, Vol. 54, No. 10, 3751–3764, Oct. 2006.

[7] Chu, Q.-X. and X.-K. Tian, "Design of UWB bandpass filter using stepped-impedance stub-loaded resonator," *IEEE Microwave and Wireless Components Letters*, Vol. 20, No. 9, 501–503, Sep. 2010.

[8] Baik, J.-W., T.-H. Lee, and Y.-S. Kim, "UWB bandpass filter using microstrip-to-CPW transition with broadband balun," *IEEE Microwave and Wireless Components Letters*, Vol. 17, No. 12, 846–848, 2007.

[9] Ghosh, P., A. Gorai, S. Behera, and R. Ghatak, "Design of compact UWB antenna using characteristic mode analysis and its quad-port MIMO realization with novel isolation technique," *Journal of Electromagnetic Waves and Applications*, Vol. 38, No. 4, 443–459, 2024.

[10] Kumari, P., P. Sarkar, and R. Ghatak, "A multi-stub loaded compact UWB BPF with a broad notch band and extended stopband characteristics," *International Journal of RF and Microwave Computer-Aided Engineering*, Vol. 30, No. 4, e22138, 2020.

[11] Sangam, R. S. and R. S. Kshetrimayum, "Notched UWB filter using exponential tapered impedance line stub loaded microstrip resonator," *The Journal of Engineering*, Vol. 2018, No. 9, 768–772, 2018.

[12] El Bakali, H. E. O., H. Elftouh, A. Farkhsi, A. Zakriti, and M. E. Ouahabi, "Design of a super compact UWB filter based on hybrid technique with a notch band using open circuited stubs," *Advanced Electromagnetics*, Vol. 9, No. 3, 39–46, Dec. 2020.

[13] Song, Y., G.-M. Yang, and W. Geyi, "Compact UWB bandpass filter with dual notched bands using defected ground structures," *IEEE Microwave and Wireless Components Letters*, Vol. 24, No. 4, 230–232, Apr. 2014.

[14] Ghazali, A. N., M. Sazid, and S. Pal, "A miniaturized low-cost microstrip-to-coplanar waveguide transition-based ultra-wideband bandpass filter with multiple transmission zeros," *Microwave and Optical Technology Letters*, Vol. 62, No. 12, 3662–3667, 2020.

[15] Chakraborty, P., J. R. Panda, and A. Deb, "Design of a novel stub loaded asymmetric rectangular ring resonator based ultra-wide notched-band bandpass filter," *Journal of Electromagnetic Waves and Applications*, Vol. 36, No. 18, 2614–2627, 2022.

[16] Chakraborty, P., J. R. Panda, A. Deb, S. Sahu, and J. S. Roy, "Design of a miniaturized split-ring resonator based UWB notched bandpass filter," *Progress In Electromagnetics Research C*, Vol. 134, 27–38, 2023.

[17] Shome, P. P., T. Khan, S. K. Koul, and Y. M. M. Antar, "Compact UWB-to-C band reconfigurable filtenna based on elliptical monopole antenna integrated with bandpass filter for cognitive radio systems," *IET Microwaves, Antennas & Propagation*, Vol. 14, No. 10, 1079–1088, 2020.

[18] Neogi, A. and J. R. Panda, "A miniaturised negative group delay triple pass band filter using half wavelength meander step impedance resonator," *Progress In Electromagnetics Research Letters*, Vol. 101, 55–62, 2021.

[19] Sharma, R. K. and M. Arora, "Meander line EBG based multiband antenna for WLAN and WiMAX application," *International Journal of Modern Communication Technologies & Research (IJMCTR)*, Vol. 5, No. 11, 265099, 2017.

[20] Elamin, N. I. M., T. A. Rahman, and A. Y. Abdulrahman, "New adjustable slot meander patch antenna for 4G handheld devices," *IEEE Antennas and Wireless Propagation Letters*, Vol. 12, 1077–1080, 2013.

[21] Lee, T.-H., K.-C. Yoon, and K. G. Kim, "Miniaturized dual-band bandpass filter using T-shaped line based on stepped impedance resonator with meander line and folded structure," *Electronics*, Vol. 11, No. 2, 219, 2022.

[22] Ansys Inc., "HFSS: High Frequency Structure Simulator, ver. 13," Canonsburg, PA, USA, 2010.

[23] Zhu, L., S. Sun, and R. Li, *Microwave Bandpass Filters for Wideband Communications*, John Wiley & Sons, 2011.

[24] Zheng, X., Y. Pan, and T. Jiang, "UWB bandpass filter with dual notched bands using T-shaped resonator and L-shaped defected microstrip structure," *Micromachines*, Vol. 9, No. 6, 280, 2018.

[25] Weng, M.-H., C.-W. Hsu, S.-W. Lan, and R.-Y. Yang, "An ultra-wideband bandpass filter with a notch band and wide upper band-stop performances," *Electronics*, Vol. 8, No. 11, 1316, 2019.

[26] Xu, Z., "UWB bandpass SSL filter with an adjustable notched band and four transmission zeros," *Electronics Letters*, Vol. 57, No. 24, 930–932, 2021.

[27] Udhayanan, S. and K. Shambavi, "Compact single notch UWB bandpass filter with metamaterial and SIW technique," *Progress In Electromagnetics Research Letters*, Vol. 117, 41–46, 2024.

[28] Wei, G., Y. X. Wang, J. Liu, Y. Gao, and X. T. Yao, "Highly selective UWB BPF with dual notched bands using split ring resonator," *Progress In Electromagnetics Research C*, Vol. 136, 51–60, 2023.

[29] Louazene, H., M. Challal, and M. Boulakroune, "Design and fabrication of a compact UWB BPF with notch-band and wide stop-band using dual MMRs and DGS," *Progress In Electromagnetics Research Letters*, Vol. 109, 75–83, 2023.

[30] Zhao, G., C. Li, M. Li, P. Zhang, Y. Yan, X. Mo, and Z. Tu, "A novel miniaturized image rejection bandpass filter basing on stepped-impedance resonators," *Progress In Electromagnetics Research Letters*, Vol. 112, 27–34, 2023.

[31] Ji, W., H. Du, Y. Tong, X. Ji, and L. Feng, "Filter design based on multilayer wide side coupling structure," *Progress In Electromagnetics Research M*, Vol. 128, 31–39, 2024.

[32] Ahmed, H. S. and A. N. Almamori, "Design of a triple-band metamaterial bandpass filter utilizing modified-minkowski fractal geometry," *Progress In Electromagnetics Research C*, Vol. 154, 159–167, 2025.